LANGMUIR



Interfaces: Adsorption, Reactions, Films, Forces, Measurement Techniques, Charge Transfer, Electrochemistry, Electrocatalysis, Energy Production and Storage

# Rational Design of Yolk-Shell CuO/Silicalite-1@mSiO2 Composites for High-Performance Non-Enzymatic Glucose Biosensor

Xiaowei Cheng, Haochen Zhao, Wenfeng Huang, Jinyang Chen, Shixia Wang, Jun-Ping Dong, and Yonghui Deng

*Langmuir*, **Just Accepted Manuscript** • DOI: 10.1021/acs.langmuir.8b01051 • Publication Date (Web): 05 Jun 2018



ACS Publications

is published by the American Chemical Society. 1155 Sixteenth Street N.W., Washington, DC 20036

# Rational Design of Yolk-Shell CuO/Silicalite-1@mSiO$_2$ Composites for High-Performance Non-Enzymatic Glucose Biosensor

Xiaowei Cheng,[1] Haochen Zhao,[2] Wenfeng Huang,[3] Jinyang Chen,[3] Shixia Wang,[2] Junping Dong,[4,5,*] and Yonghui Deng[1,5,*]

[1] Department of Chemistry, State Key Laboratory of Molecular Engineering of Polymers, Shanghai Key Laboratory of Molecular Catalysis and Innovative Materials, iChEM (Collaborative Innovation Center of Chemistry for Energy Materials), Fudan University, Shanghai 200433, China.

[2] College of Science, University of Shanghai for Science and Technology, Shanghai 200093, China.

[3] School of Environmental and Chemical Engineering, Shanghai University, Shanghai 200444, China.

[4] Department of Chemistry, College of Science, Shanghai University, Shanghai 200444, China.

[5] State Key Lab of Transducer Technology, Shanghai Institute of Microsystem and Information Technology, Chinese Academy of Sciences, Shanghai 200050, China.

*KEYWORDS yolk-shell, CuO/silicalite-1@mSiO2, mesoporous silica, electrocatalyst, non-enzymatic, glucose biosensor*

**ABSTRACT:** In this study, an interface coassembly strategy is employed to rationally synthesize yolk-shell CuO/silicalite-1@void@mSiO$_2$ composite consisting of silicalite-1 supported CuO nanoparticles confined in the hollow space of mesoporous silica, and the obtained composite materials were used as a novel non-enzymatic biosensor for highly sensitive and selective detecting glucose with excellent anti-interference ability. The synthesis of CuO/silicalite-1@mSiO$_2$ include four steps, coating silicalite-1 particles with resorcinol-formaldehyde polymer (RF), immobilization of copper species, interface deposition of a mesoporous silica layer, and final calcination in air to decompose RF and form CuO nanoparticles. The unique hierarchical porous structure with mesopores and micropores are beneficial to selectively enrich glucose for fast oxidation into gluconic acid. Besides, the mesopores in silica shell can effectively inhibit the large interfering substances or biomacromolecules diffusing into the void as well as the loss of CuO nanoparticles. The hollow chamber inside serves as a nanoreactor for glucose oxidation catalyzed by the active CuO nanoparticles, which are spatially accessible for glucose molecules. The non-enzymatic glucose biosensors based on CuO/silicalite-1@mSiO$_2$ materials show the excellent electrocatalytically sensing performance with a wide linear range (5 ~ 500 μM), high sensitivity (5.5 μA·mM$^{-1}$·cm$^{-2}$), low detection limit (0.17 μM), and high selectivity against interfering species. Furthermore, the unique sensors even display a good capability in the determination of glucose in real blood serum samples.

## ■ INTRODUCTION

In recent years, inorganic porous solids with hierarchical pore structures have attracted great interests of researchers, because they contain structurally well-defined pore systems, and spatially accessible and exposed active centers, which offer many opportunities for designing new heterogeneous catalysts, adsorbents and functional materials.[1] Zeolites are the typical crystalline microporous materials (pore size < 2 nm) with high thermal stability, precise shape selectivity and controllable surface acidity, so they are widely used as heterogeneous catalysts or catalyst supports in large-scale industrial applications.[2] Recently, fabrication of hierarchical zeolites through various pathways has attracted much attention, with the purpose of overcoming the serious diffusion restriction of large molecules inside zeolite micropores and creating some new synergetic functions derived from bimodal or trimodal pore structures as well.[3,4] Mesoporous silica is one of the most promising porous materials, with uniform interconnected mesopores (pore size > 2 nm) and numerous outstanding peculiarities.[5,6] Therefore, it's highly expected that the ideal hierarchical pore structures should combine both micropores and mesopores in a composite entity consisting of zeolites and mesoporous silica.[3,4] Among these hierarchical composites, the porous solid materials with core-shell structures attracted particular interests due to their unique and well-arranged multimodal pore structures,[7,8] in which mesoporous silica acts as a shell covering the crystalline zeolite core. The desired multifunctional materials with core-shell structures and different morphologies or compositions can provide pow-

erful platforms for many applications in nanocatalysis,[9,10] biofunctional materials,[11,12] energy storage and conversion,[13] and so on. Yoon and co-workers synthesized core-shell silicalite-1@mesoporous silica for the first time, in which the shell was composed of disordered wormlike mesoporous silica.[14] Through leaching of silicate species from zeolite Y in an ammonia solution and simultaneous in-situ assembly of mesoporous silica using the dissolved silicate species as silica source, Han et al. reported a one-pot method for the preparation of core-shell zeolite Y@mesoporous silica.[15] Furthermore, Zhao group has also fabricated a series of core-shell composite molecular sieves, in which zeolite single crystals were used as the core covered by the uniform shell of ordered mesoporous silica with perpendicular pores.[16-19]

The yolk-shell nanocomposites are a special class of core-shell materials with rattle-type structures of core/void@shell configuration, which are generally composed of distinctively movable cores, interstitial hollow space and functionalized porous shells.[20] These composite materials are reported to present unique structural configurations: the solid core acts as a support to disperse nanoparticles or anchor guest biomolecules, the tunable hollow space provides enough accommodation for reactant molecules as a nanoreactor,[20] and the outer shell plays a molecular-sieving role or protects the core from surrounding environment.[21-23] Therefore, the yolk-shell functional materials pave a powerful platform for successful application in lithium-ion batteries,[23] catalysts,[24] biosensors,[25] drug or DNA/siRNA delivery,[26,27] surface-enhanced Raman scattering[28] and so on. Our group has designed the novel yolk-shell microspheres consisting of magnetic cores and mesoporous silica shells ($Fe_3O_4$@mSiO2) supported Au nanoparticles, which can be easily recycled with a magnetic field, and reused without significant reduction of catalytic activity even after recycled use for 12 times.[20] To the best of our knowledge, when zeolites are used as the heterogeneous catalysts, one of the most important features is to precisely control the textural properties as well as the adjustable surface acidity.[29] Despite that the mesoporous silica shell in the core-shell composites owns perpendicular open channels connecting with the inner zeolite core, the surface acidity and micropore sorption are inevitably reduced by partial blocking and coverage of amorphous silica species.[7,8,14-19] Therefore, the composite molecular sieves with rattle-like structure are promising to solve these obstacles, because the mesoporous silica shell is not in contact with zeolite surface, leading to the commendable maintenance of intrinsic textural properties and surface acidity of zeolite as well as the huge void for the subsequent application. But until now, there have not been any reports about the synthesis of yolk-shell zeolite@mesoporous silica molecular sieves. Different from the core-shell zeolite@mesoporous silica composites reported before,[7,8,14-19] a huge hollow chamber is created in our designed yolk-shell ones, which could provide the wide-open nanospace for loading enzymes or nanoparticles of metal or metal oxide, catalytic reactions, etc.[20,30]

The accurate and fast detection of glucose is of great significance in biotechnology, food industry and clinical diagnosis, therefore, glucose biosensors have always been attracting considerable attention.[31-33] Although the glucose oxidase-based electrochemical biosensors own high sensitivity and selectivity, they suffer drawbacks including poor stability and high cost.[34] Hence, it is of great interest and importance to develop non-enzymatic glucose biosensors which are based on the catalysts of metal (e. g. Au, Pt, Pd, Cu, Ni), metal oxide (e. g. $Co_3O_4$, NiO, CuO) or alloy (Pt/Pb, Pt/Au, Au/Ag).[34] The metal oxides, such as $Co_3O_4$,[35] NiO,[36] CuO,[37,38] have been demonstrated to exhibit high catalytic activity in glucose electro-oxidation. As one of the important *p*-type semiconductors, CuO as the electrocatalyst has gained increasing concerns for its low cost, high stability, good electrical conductivity and easy availability, which also possesses notable electrocatalytic activity in oxidation of glucose.[34,39-41] However, it still remains a great challenge to control the aggregation of CuO nanoparticles in preparation and electrocatalytic reaction as well as enhance the sensitivity, stability, selectivity and anti-interference ability as a commercialized biosensor applied in complex physiological systems.

Herein, through a facile sol-gel interface coassembly strategy, the yolk-shell CuO/silicalite-1@mSiO2 molecular sieves (denoted as CuO/S-1@mSiO2) were prepared for the first time, which were then used as a highly active electrocatalyst for glucose oxidation in a non-enzymatic glucose biosensor. The hierarchical pore structures of mesopores and micropores can selectively adsorb glucose and oxidation product of gluconic acid, respectively. Besides, the mesopores in silica shell play a molecular sieving role in restricting the diffusion of interfering substances or biomacromolecules into the hollow void as well as preventing the loss of CuO. Ultrafine CuO nanoparticles, stably dispersed on the surface of silicalite-1 within the hollow chamber, are spatially accessible for glucose molecules enriched by mesoporous silica shell and show high catalytic activity in glucose oxidation. Therefore, the yolk-shell CuO/S-1@mSiO2 based non-enzymatic glucose biosensor exhibits the excellent performance in glucose detection, such as high sensitivity, low detection limit, good selectivity and strong anti-interference ability. The glucose concentration in real human serum sample was also determined by our biosensor, showing good accuracy and high precision.

## ■ EXPERIMENTAL

### 1 Chemicals and materials

Tetraethylorthosilicate (TEOS), resorcinol, formaldehyde, ethanol, and concentrated ammonia solution (28 wt%) in analytical grade were supplied by Shanghai Chemical Corp. (China). The reagents of [N-(2-aminoethyl)-3-aminopropyl]-trimethoxysilane (AAPTMS) (97%), cetyltrimethyl ammonium bromide (CTAB), tetrapropylammonium hydroxide (TPAOH, 40%), uric acid (UA), ascorbic acid (AA) and dopamine (DA) were bought from Sigma-Aldrich. Human serum samples (from female O plasma) were supported by the Changhai hospi-

tal (Shanghai, China). The other reagents of $CuSO_4 \cdot 5H_2O$, NaOH, NaCl, glucose, fructose and sucrose were provided by Sinopharm Chemical Reagent Co., Ltd. (China).

## 2 Procedure for the preparation of yolk-shell CuO/S-1@mSiO2 composites

### 2.1 Synthesis of silicalite-1 single crystals

The all-silica MFI zeolite, also named as silicalite-1 (S-1), was synthesized by the hydrothermal crystallization method. The molar composition of the synthesis mixture was $1SiO_2$:0.25TPAOH:4ethanol:$46H_2O$. The typical synthesis was undertaken as follows: 3.18 mL of TPAOH solution was added into 19.48 mL of deionized water. Then, 5.57 mL of TEOS was added dropwise in the diluted TPAOH solution during 10 min under constant stirring. After being stirred at 35°C for 5 h, the gel was transferred into a 50 mL Teflon-lined steel autoclave and crystallized at 170°C for 3 days. The product was recovered by centrifugation, washed with deionized water and dried overnight at 80°C.

### 2.2 Synthesis of core-shell S-1@RF particles and immobilization of $Cu^{2+}$

The S-1 single crystals of 0.16 g synthesized before were dispersed in a solution of ethanol (80 mL) and deionized water (40 mL) by ultrasonication, then 2.5 mL ammonia solution, 0.30 g resorcinol and 0.42 mL formaldehyde were consecutively added into the mixture. The S-1 containing dispersions were mechanically stirred at 35°C for 12 h, resulting in the coating of a polymeric resorcinol-formaldehyde shell on the surface of S-1, so that the sample was denoted as S-1@RF. After that, the S-1@RF particles were collected by centrifugation, and then washed with deionized water and ethanol for three times respectively, finally dried at 60°C for 12 h. The thickness of RF layers on S-1 crystals were controlled by tuning the amount of ammonia solution, resorcinol and formaldehyde correspondingly. The amine-functionalized S-1@RF was prepared by a post-synthetic grafting method. In a typical process, AAPTMS in excess amount of 0.30 g was added into S-1@RF of 0.1 g in anhydrous toluene, which was sequentially stirred at room temperature for 24 h under argon atmosphere. The resulting solid particles were centrifuged, washed with toluene, dried under vacuum at 50°C overnight, and then stored in a dry box for further use. At last, 0.10 g amine-functionalized S-1@RF powder was dispersed in 25 mL of $CuSO_4$ solution (0.1 mol/L) for stirring at 25°C for 12 h. After that the centrifugation and washing with deionized water were conducted several times to remove uncoordinated $CuSO_4$. The content of $Cu^{2+}$ in amine-functionalized S-1@RF could be controlled by the concentrations of $CuSO_4$ aqueous solution (0 ~ 0.2 mol/L).

### 2.3 Synthesis of yolk-shell CuO/S-1@mSiO2 composites

Mesoporous silica was coated on the surface of S-1@RF-$Cu^{2+}$ particles by a classical Stöber method. In a typical synthesis, the S-1@RF-$Cu^{2+}$ particles (0.04g) were first dispersed in a mixed solution containing CTAB (0.099 g), deionized water (35 mL), ethanol (45 mL) and concentrated ammonia solution (0.5 mL) by ultrasonication treatment. Subsequently, 0.2 mL of TEOS was added into the solution drop by drop within 10 min. The whole synthesis was carried out under stirring at 25°C for 6 h. The product was collected by centrifugation and washed with ethanol and deionized water for several times. Finally, the target product of yolk-shell CuO/S-1@mSiO2 was obtained by calcination in air with a heating rate of 5°C/min and maintained at 650°C for 6 h. For comparison, the sample of CuO/S-1 was obtained by direct calcination of S-1@RF-$Cu^{2+}$ under the same conditions.

## 3 Fabrication of CuO/S-1@mSiO2 modified glassy carbon electrode

The glassy carbon electrode (GCE, 3 mm in diameter) was polished with 0.3 μm and 0.05 μm $Al_2O_3$ powders sequentially, followed by thorough rinsing with deionized water. After ultrasonication in deionized water, ethanol, and deionized water in sequence, the GCE with clean surface was dried at room temperature. The yolk-shell CuO/S-1@mSiO2 was dispersed into double distilled water and grinded to form suspension of 2 mg/mL. Approximately 8 μL of the suspension and 4 μL of 0.5% Nafion (Alfa Aesar) were dropped onto the surface of GCE uniformly and dried under irradiation of infrared lamp.

## 4 Characterizations

Powder X-ray diffraction (XRD) patterns were recorded on a Bruker D4 X-ray diffractometer (Germany) with Ni-filtered CuKα radiation (40 kV, 40 mA). Field-emission scanning electron microscopy (FESEM) images were collected on the Hitachi Model S-4800 field emission scanning electron microscope (Japan). Transmission electron microscopy (TEM) experiments were conducted on a JEOL 2011 microscope (Japan) operated at 200 kV. Elemental mapping and energy-dispersive spectroscopy (EDS) were performed with the high-resolution transmission electron microscopy (HRTEM) measurements on a JEOL JEM-2100F microscope (Japan) operated at 200 kV. FT-IR spectra were obtained on an Avater 370 FTIR spectrograph (Nicolet Co., USA) by a KBr tabletting method. Nitrogen sorption isotherms were measured at 77 K with a Micromeritics ASAP 2020 analyzer. Before measurements, all the samples were degassed in a vacuum at 180°C for at least 12 h. The surface area and mesopore size distribution were calculated by Brunauer-Emmett-Teller (BET) and Barrett-Joyner-Halenda (BJH) methods, respectively. The micropore surface area and volume were calculated by a *t*-plot method. The external pore volumes were obtained from the BJH adsorption cumulative volume of pores between 1.7 and 300 nm in diameter. All electrochemical experiments were performed on CHI 660C electrochemical workstation (Chenhua, Shanghai, China) with a conventional three-electrode system, in which the bare GCE or modified GCE was served as the working electrode, an Ag/AgCl (3 M KCl) electrode acted as the reference one and the platinum wire was used as the auxiliary electrode. Cyclic voltammetry (CV) was carried out between 0 V and +0.7 V at a scan rate of 50 mV/s. All the electrochemical experiments were conducted at room

temperature and were repeated at least three times to verify the reproducibility.

## ■ Results and discussion

The zeolite of silicalite-1 in average size of 240~260 nm was synthesized by a hydrothermal method, which is a kind of all-silica MFI zeolite with controllable morphology and surface properties and widely used as the adsorbent or catalyst in industry. The morphology and surface properties of silicalite-1 could be well controlled, which can be modified with RF coating uniformly to get the core-shell silicalite-1@RF composite. The as-made silicalite-1 sample after washing and drying was directly used as a core for follow-up fabrications of core-shell or yolk-shell composites. The micropores of silicalite-1 are still occupied by $TPA^+$ cations as the template after drying at 80°C. Without calcination the intrinsic properties, such as surface silanol groups and hydrophilicity, could be well maintained, which are beneficial to uniform assembly of RF resin on silicalite-1 through interaction of hydrogen bonds. Figure 1 presents the scheme of multistep assembly process for CuO/S-1@mSiO2 composites with yolk-shell structures. Firstly, template-containing silicalite-1 crystals were coated with a protective RF shell through the interface sol-gel polymerization of resorcinol and formaldehyde under alkaline conditions, to obtain the core-shell S-1@RF hybrid composites. Secondly, through the successive impregnation grafting method, RF surface was modified with amino groups by the agent of AAPTMS, and then $Cu^{2+}$ could be stably immobilized on this amino-functioned S-1@RF via coordination of $Cu^{2+}$ with amino groups. Thirdly, a thin layer of CTAB/silica mesostructured composites was deposited on S-1@RF-$Cu^{2+}$ through an interface coassembly strategy using TEOS as a silica source and CTAB as a template, conducted in an ultra-dilute alkaline solution under stirring. Finally, organic components of TPAOH, CTAB and AAPTMS were removed by calcination under air flow in one step, and $Cu^{2+}$ was converted into CuO in this process. The obtained yolk-shell composites with CuO coordinated in hollow void were denoted as CuO/S-1@mSiO2.

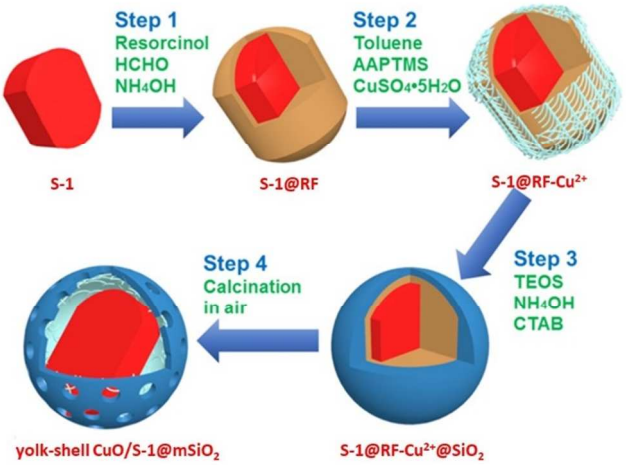


**Figure 1.** Schematic assembly process of the yolk-shell CuO/S-1@mSiO2 composites. Step 1: formation of core-shell inorganic-organic hybrid composites of S-1@RF by coating polymeric resorcinol formaldehyde (RF) on silicalite-1 (S-1). Step 2: amino-functioned treatment with AAPTMS and surface modification with $Cu^{2+}$ by impregnation grafting method to obtain S-1@RF-$Cu^{2+}$. Step 3: growth of mesoporous silica as a shell using CTAB as a template by a sol-gel coassembly method for S-1@RF-$Cu^{2+}$@SiO2 composite particles. Step 4: the yolk-shell CuO/S-1@mSiO2 obtained by calcination in air to remove all organic components and form CuO nanoparticles in one step.

Figure 2 presents X-ray diffraction (XRD) patterns of the as-synthesized silicalite-1, core-shell S-1@RF and yolk-shell CuO/S-1@mSiO2 composites, respectively, all of which have the characteristic diffraction peaks assigned to the typical topology structures of MFI zeolite with high crystallinity. After coating a shell of RF resin or mesoporous silica on silicalite-1 (Figure 2a), the peak intensities of S-1@RF (Figure 2b) and CuO/S-1@mSiO2 (Figure 2c) slightly decline, mainly because of shielding effects of amorphous species of RF resin or silica as a thin shell. The typical diffraction peaks at 32.5°, 35.4° and 38.7°/2θ can be exactly indexed to (110), (002) and (111) lattice planes of crystalline CuO with tenorite phase (monoclinic, PDF05-0661), respectively (Figure S1).[41] The content of Cu loaded in CuO/S-1@mSiO2 is determined to be 1.83% by energy-dispersive spectroscopy (EDS), higher than the detection limit of XRD, but the diffraction peaks of crystalline CuO particles cannot be found (Figure S1-c). The fact may be explained by the general distinguishing features as the ultrafine CuO nanoparticles and the shielding effects of mesoporous silica shell. No diffraction peaks arise in the small-angle XRD pattern of CuO/S-1@mSiO2 (Figure S2), showing that disordered mesostructures probably form in the silica shell by sol-gel coassembly process in our synthesis.

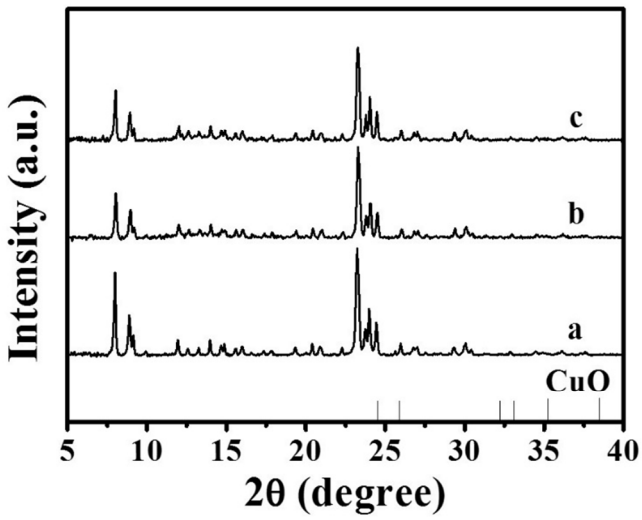


**Figure 2.** XRD patterns of (a) as-made silicalite-1, (b) core-shell S-1@RF with shell thickness of 50 nm, and (c) yolk-shell CuO/S-1@mSiO2 with 1.83 wt% copper and shell thickness of 100 nm, respectively.

Fielding-emission scanning electron microscopy (FESEM) image of the as-made silicalite-1 (Figure 3a) shows numerous monodispersed crystals with regular

hexagonal prism morphology, each of that owns rough surface and uniform crystal dimension of about 250×250×125 nm. The corresponding transmission electron microscopy (TEM) image of silicalite-1 in Figure 3b also exhibits the analogous observations in crystal size and morphology, providing appropriate interface for sol-gel polymerization of resorcinol and formaldehyde. After coating a RF resin shell, the obtained inorganic-organic hybrid particles still remain highly dispersed and uniform in size and morphology (Figure 3c and 3d). The core-shell S-1@RF particles also show the quasi hexagonal prism morphology similar with silicalite-1, in larger dimensions of around 350×350×220 nm; however, the RF shell possesses the relatively round outer surface with obtuse edges, in order to achieve the minimum surface energy in sol-gel interface coassembly.[42] Since no template such as CTAB was used in the coating process, the polymeric RF layer in thickness of approximately 50 nm has dense structures without mesopores inside (inset in Figure 3d), which could well protect the silicalite-1 core from surrounding alkaline environment in successive fabrications and provide the active surface for amino modification and $Cu^{2+}$ grafting. Through changing the amount of resorcinol and formaldehyde, the thickness of RF shell can be precisely adjusted from 20 nm to 65 nm (Figure S3), which will dominate the space of hollow chamber in the final yolk-shell sample of CuO/S-1@mSiO2. Interestingly, the S-1@RF chains with different RF thickness and chain length are obtained (Figure S3, a-c), depending on the morphology and aggregation of silicalite-1 crystals and honestly making a precise copy of their profiles. When the shell thickness increases up to 65 nm, some segregative RF microspheres about 100 nm in diameter are formed in adhesion to the surface of S-1@RF particles (Figure S3-d), which probably emerge from fast heterogeneous nucleation of RF microspheres in solution containing superfluous resorcinol and formaldehyde.

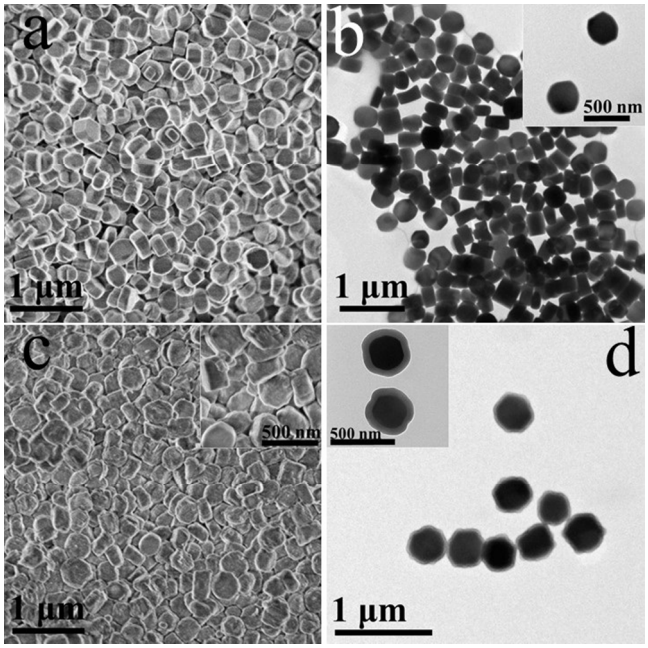


**Figure 3.** FESEM and TEM images: (a, b) pristine silicalite-1 single crystals showing a crystal dimension of about 250×250×125 nm with hexagonal prism morphology and rough external surface. (c, d) uniform core-shell S-1@RF particles with shell thickness of 50 nm synthesized by a sol-gel polymerization strategy.

In order to prohibit the generation of $Cu(OH)_2$ precipitates in alkaline sol-gel system for coating mesoporous silica shell, and enhance the stability and dispersity of copper species as well, an impregnation grafting route was carried out to modify RF resin with amino groups, through condensation reaction of hydroxyl groups (-OH) in RF with methoxyls ($CH_3O$-) in AAPTMS. The absorption peaks at 1609 $cm^{-1}$ and 552 $cm^{-1}$ in FT-IR spectrum (Figure S4), assigned to the stretching of N-H bonds,[43] prove the successful grafting of amino groups on RF resin. After coating a mesoporous silica shell on S-1@RF-$Cu^{2+}$ with calcination, the obtained CuO/S-1@mSiO2 particles are less uniform and dispersed than S-1@RF (Figure 4a). The hexagonal prism morphology of silicalite-1 is almost changed after coating a silica layer, which turns to quasi microspheres with irregular shapes in larger size of 550 nm to 600 nm (Figure 4b). Nearly no separated silica spheres are generated in the coating process, indicating that the heterogeneous nucleation of silica into microspheres could be forbidden in a dilute solution. Otherwise, the homogeneous sol-gel coassembly of silica primarily performs on the interface of copper-coating amino-functioned RF resin. TEM images in Figure 4c and 4d display the well-distributed composite molecular sieve particles with a specific yolk-shell structure, which are composed of silicalite-1 crystal as a core, large hollow void and mesoporous silica as a shell. FESEM image of a cracked CuO/S-1@mSiO2 particle clearly reveals the typical yolk-shell structure (Figure 4a, inset), indicating that the CTAB-directed sol-gel coassembly strategy is suited to silica coating as a mesoporous shell to form core-shell or yolk-shell composite molecular sieves.[44] The thickness of mesoporous silica shell is uniform and estimated to be approximately 100 nm (Figure 4c and 4d), which can be tailored from 50 nm to 150 nm by changing the ratio of TEOS to S-1@RF/$CuSO_4$. Whereas, when the thickness is below 50 nm, the silica shell is quite fragile and easy to be broken with great shrinkage by calcination, leading to the complete disappearing of the hollow void created by RF (Figure S5-a and b). When more TEOS was added dropwise into the coating system, the shell thickness could be increased to 150 nm in maximum (Figure S5-c), but a great number of separated silica microspheres in size of about 600 nm are produced due to phase separation and fast heterogeneous nucleation of silica source at high concentration (Figure S5-d). With a core of silicalite-1 single crystal in size of 250 nm, the diameter of hollow void in CuO/S-1@mSiO2 is sized up to be about 500 nm to 600 nm (Figure 4c and 4d), which is consistent with the diameter of S-1@RF (Figure 3d), implying that the hollow void comes into being from RF removal, and silicalite-1 core and mesoporous silica shell of 100 nm in thickness remain highly rigid without severe shrinkage or damage under calcination. TEM images (Figure 4e and 4f) reveal that a large number of worm-like disordered meso-

pores created by CTAB as a template are well distributed in the silica shell, in consistence with the observation in small-angle XRD (Figure S2), which could provide a close connection pathway between the exterior of mesoporous silica shells and the interior of hollow voids. No separated bulky CuO particles are observed in TEM images of all samples (Figure 4 and S5), proving that the coordination interaction between copper species and amino groups on RF resin successfully inhibits the growth of individual CuO particles. The image of high-angle annular dark-field (HAADF)-STEM in Figure 5a also clearly shows the yolk-shell structures of CuO/S-1@mSiO2 with a core of silicalite-1 in size of about 250 nm, a large hollow void and a uniform mesoporous silica shell in thickness of 100 nm. The element mappings demonstrate that Si and O elements are regularly distributed in silicalite-1 core and mesoporous silica shell (Figure 5c and 5d), however, most of the copper elements are dispersed around the surface of silicalite-1 in the hollow chamber (Figure 5e), and few of them diffuse inside the mesopores in the silica shell probably driven by calcination (Figure S6). The copper content is calculated to be 1.83 % (Figure 5b and Table S2), further confirming the regular yolk-shell configuration of CuO/S-1@mSiO2 with uniform immobilization of ultrafine CuO nanoparticles in the hollow void.

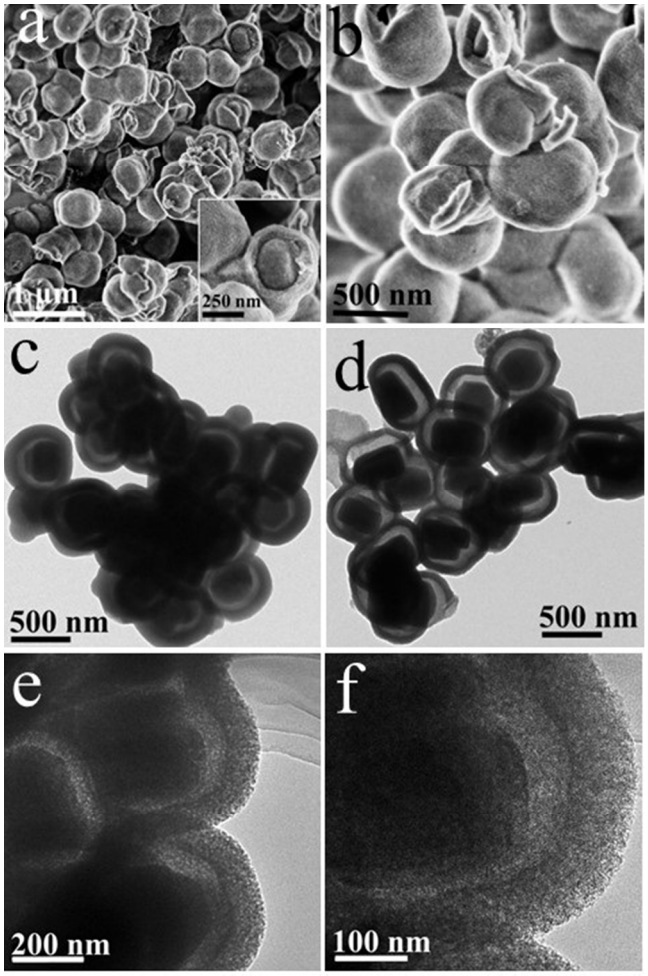


**Figure 4.** FESEM images (a, b) and TEM images (c, d, e, f) of the yolk-shell CuO/S-1@mSiO2 composites with 1.83 wt% copper prepared by CTAB-directed sol-gel coating strategy showing uniform shell thickness of 100 nm and mesopores in the shell structure.

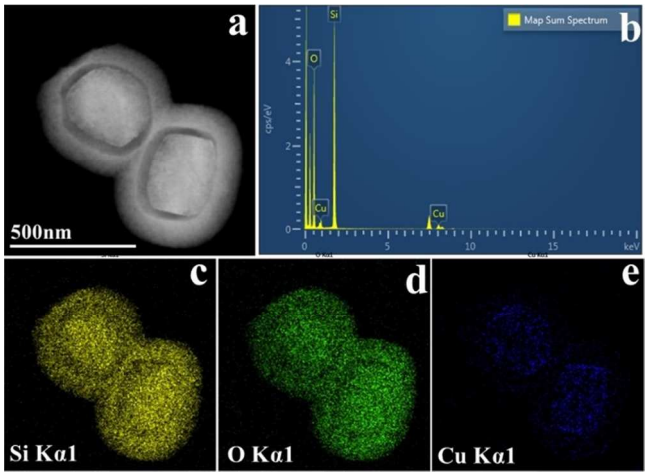


**Figure 5.** (a) HAADF-STEM image of the yolk-shell CuO/S-1@mSiO2 composites with 1.83 wt% copper prepared by CTAB-directed sol-gel coating strategy showing uniform shell thickness of 100 nm, its corresponding EDS (b) and element mapping of silicon (c), oxygen (d) and copper (e).

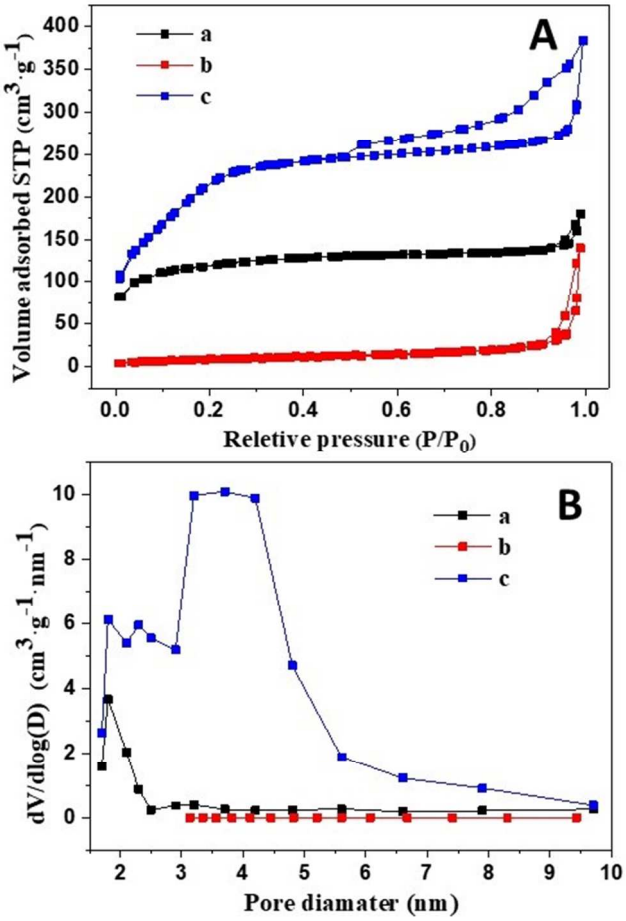


**Figure 6.** (A) Nitrogen sorption isotherms (B) pore size distribution curves of (a) silicalite-1 after calcination, (b) as-made core-shell S-1@RF with shell thickness of 50 nm, and (c) yolk-shell CuO/S-1@mSiO2 with 1.83 wt% copper and shell thickness of 100 nm, respectively.

Nitrogen sorption isotherms of silicalite-1 (after calcination) present a characteristic type-I curve with a sharp

uptake at low relative pressure ($P/P_o$), corresponding to the intrinsic microporous structures of zeolite materials (Figure 6A-a). Its specific BET surface area and total pore volume are 353 $m^2/g$ and 0.267 $cm^3/g$ (Table S1), respectively, with a low contribution of external surface or mesopores (34 $m^2/g$ and 0.095 $cm^3/g$). Whereas, the nitrogen adsorption volume of S-1@RF almost decreases to zero at low $P/P_o$ (Figure 6A-b). Its BET surface area and total pore volume are as low as 9 $m^2/g$ and 0.065 $cm^3/g$ (Table S1), respectively, which are mainly from the contributions of external surface, due to blocking of micropores in silicalite-1 by un-removed TPAOH and coated dense RF shell in thickness of 50 nm. After fabrication of mesoporous silica shell, the nitrogen sorption isotherms of CuO/S-1@mSiO2 with yolk-shell structure in Figure 6A-c display a steep uptake at low $P/P_o$ (type I curve for microporous materials) and a capillary condensation step at middle $P/P_o$ (type IV curve for mesoporous materials) as well as a distinct H2-type hysteresis loop, demonstrating the perfect combination of micropores and cage-like mesopores in one composite material. The BET surface area and total pore volume of CuO/S-1@mSiO2 increase up to 779 $m^2/g$ and 0.416 $cm^3/g$, respectively, with about 466 $m^2/g$ of surface area and 0.245 $cm^3/g$ of pore volume stemming from the contributions of mesopores in silica shell (Table S1), and the average pore size is determined to be around 4 nm (Figure 6B-c). Remarkably, its microporous surface area and volume are 313 $m^2/g$ and 0.171 $cm^3/g$, respectively, which are mainly from the core and slightly lower than those of pristine silicalite-1, indicating that most micropores in silicalite-1 remain open, which are not blocked by loaded CuO nanoparticles or coated silica shell.

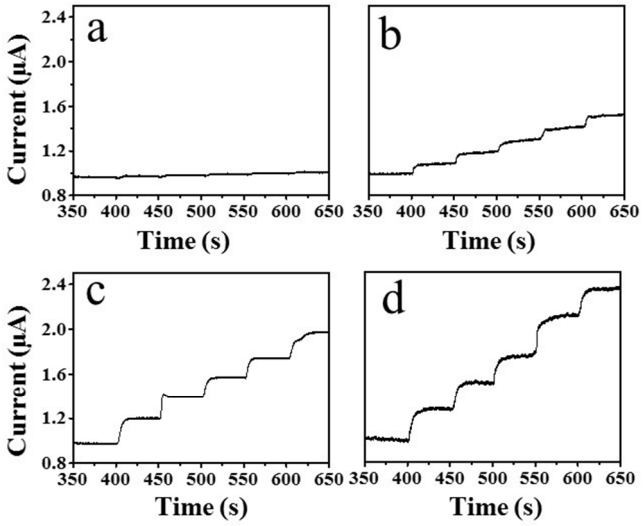


**Figure 7.** Amperometric responses of the glassy carbon electrode modified by yolk-shell CuO/S-1@mSiO2 samples in shell thickness of 100 nm with different copper contents of (a) 0, (b) 0.37%, (c) 1.83%, and (d) 2.05% to 0.5 mM glucose in 0.1 M NaOH solution at applied potential of 0.65 V, respectively.

According to the particular yolk-shell molecular sieve structures with completely open hierarchical mesopores and micropores, huge hollow chamber inside and spatially accessible ultrafine CuO nanoparticles, the quantitative detection of glucose was conducted on a glass carbon electrode (GCE) modified by yolk-shell CuO/S-1@mSiO2 as a non-enzymatic biosensor using amperometry method. As reported in our previous work,[45] electro-oxidation of glucose occurred at around 0.65 V when $Cu^{2+}$ species were used as the active catalyst. Firstly, CuO/S-1@mSiO2 modified electrodes with different copper contents are tested for comparison in Figure 7. Very weak currents (Figure 7a) indicate that nearly no oxidation reaction happens on the electrode surface, because the silicate species in silicalite-1 and mesoporous silica perform no catalytic activity in glucose electro-oxidation. With each injection of glucose into NaOH solution, the oxidation currents of glucose rise sharply, and the current value achieves 95% of the steady-state current within 4 s (Figure 7b). As copper content increasing from 0.37% to 2.05%, the response currents increase apparently with injection of the same amount of glucose (Figure 7b to 7d), proving that Cu species are the active centers for glucose electro-oxidation. The maximum of Cu loading is 2.05% due to insufficiency of amino groups coordinated with copper species. The glucose electro-oxidation of CuO/S-1@mSiO2 is mainly from the catalytic activity of CuO, which is considered as the active sites. The electrocatalytic oxidation process of glucose in the alkaline electrolyte at the CuO electrodes is generally considered undergoing several steps as follows.[45,46] Firstly, CuO is electrochemically oxidized to strong oxidizing Cu(III) species such as CuOOH or $Cu(OH)^{4-}$.

$$CuO + OH^- \rightarrow CuOOH + e^- \text{ or}$$

$$CuO + H_2O + 2OH^- \rightarrow Cu(OH)^{4-} + e^-$$

And then, glucose is catalytically oxidized by Cu(III) species to produce gluconic acid.

$$Cu(III) + \text{glucose} + e^- \rightarrow Cu(II) + \text{gluconolactone};$$

$$\text{gluconolactone} \rightarrow \text{gluconic acid (hydrolysis)}$$

Furthermore, the amperometric response of yolk-shell CuO/S-1@mSiO2 modified electrode was compared with that of CuO/S-1 with the same copper content as shown in Figure S7. Despite that CuO species are deposited on the surface of silicalite-1 in CuO/S-1, which are more accessible with glucose molecules, the electrode modified with CuO/S-1@mSiO2 shows higher response current under the same conditions (Figure S7-a). The excellent response of CuO/S-1@mSiO2 to glucose could be explained as follows. First, glucose molecules in solution can quickly diffuse into mesopores in the silica shell due to its molecular sieving role, which are then enriched in the hollow void. Second, the large chamber can provide enough reaction space for glucose oxidation as a nanoreactor, accommodate many electrolyte molecules or ions, which can freely diffuse in or out of the mesoporous silica shell. Third, ultrafine CuO nanoparticles are highly dispersed on the surface of silicalite-1 in the void, which perform as the active reaction sites and supply rich exposed interface for glucose oxidation. Forth, gluconic acid as the oxidation product, escaping from the active sites of CuO particles, quickly diffuse into the micropores of silicalite-1 by

adsorption, which can make the catalyst regenerate in situ and greatly enhance the reaction rate of glucose oxidation.

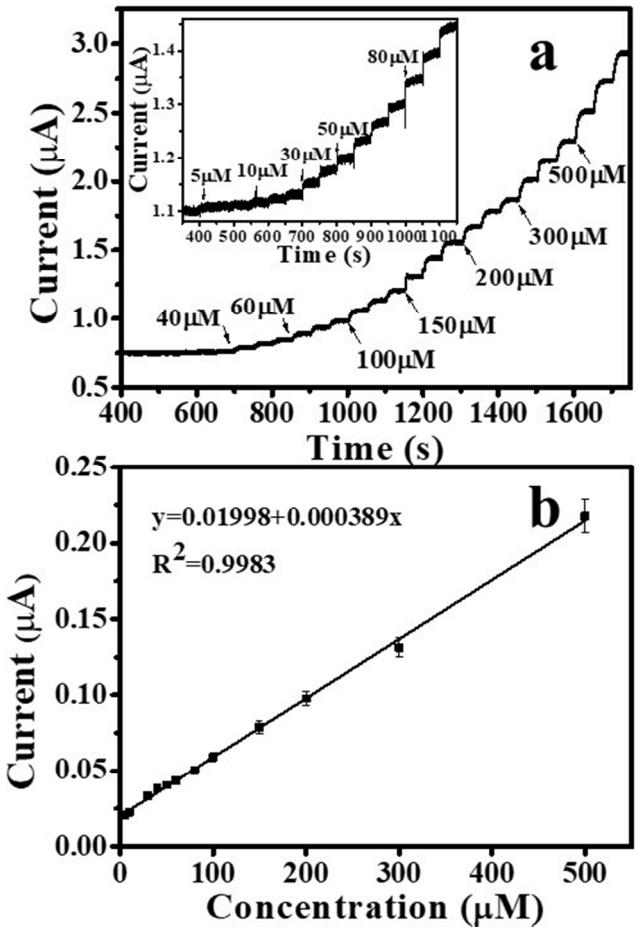


**Figure 8.** (a) Current-time responses of the glassy carbon electrode modified by yolk-shell CuO/S-1@mSiO2 with 1.83 wt% copper and shell thickness of 100 nm to the successive injections of glucose from 5 to 500 μM in 0.1 M NaOH at applied potential of 0.65 V, and (b) the corresponding calibration curve.

Figure 8 displays the current-time (I-T) curves of yolk-shell CuO/S-1@mSiO2 modified electrode to successive injections of glucose at different concentrations from 5 to 500 μM in 0.1 M NaOH electrolyte at 0.65 V. The response currents of glucose rise sharply to higher than 95% of the steady-state current in 4 s with each injection of glucose. The calibration curve for glucose detection on CuO/S-1@mSiO2 modified GCE is shown in Figure 8b. The response currents of the biosensor are linearly dependent on the concentration of glucose in the range of 5 - 500 μM with a fitting linear equation as: I (μA) = 0.01998+0.000389 $C_{glucose}$ (μM) ($R^2$=0.9983). Although the copper content is only 1.83%, the lowest in all reports, the sensitivity of the CuO/S-1@mSiO2 sensor is calculated to be 5.51 $\mu A \cdot mM^{-1} \cdot cm^{-2}$, and the detection limit is estimated to be 0.17 μM (S/N=3), exhibiting the excellent performance in terms of wide linear range and low detection limit in comparison with non-enzymatic glucose sensors based on Cu or CuO nanomaterials.[45] The good performance of CuO/S-1@$mSiO_2$ as the glucose biosensor is mainly attributed to its sophisticated yolk-shell structure.

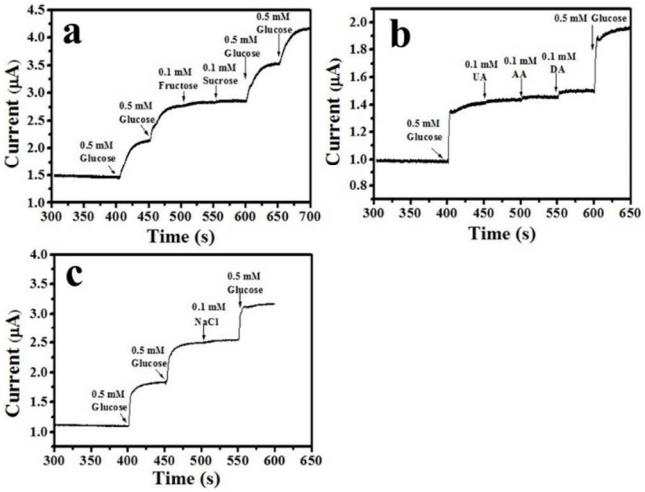


**Figure 9.** Amperometric responses of the glassy carbon electrode modified by yolk-shell CuO/S-1@mSiO2 with 1.83 wt% copper and shell thickness of 100 nm to successive injections of (a) 0.5 mM glucose, 0.1 mM fructose, 0.1 mM sucrose, (b) 0.5 mM glucose, 0.1 mM UA, 0.1 mM AA, 0.1 mM DA and (c) 0.5 mM glucose, 0.1 mM NaCl in 0.1 M NaOH electrolyte at applied potential of 0.65 V.

It's well known that the selectivity and anti-interference ability of a sensor is one of the most important factors in commercialized application for glucose detection in real physiological system since the easily oxidative species may coexist with glucose sample. Figure 9 shows the amperometric responses of the CuO/S-1@mSiO2 modified GCE to the injection of some interferential species, which are commonly present in physiological samples and may interfere with the accurate determination of glucose. Sucrose is a common type of sugars, which can be easily hydrolyzed into glucose and fructose with the same moles, so three sugars of glucose, fructose and sucrose always coexist in some specific samples. Nearly no response current could be detected after the injection of 0.1 mM fructose and 0.1 mM sucrose in 0.1 M NaOH solution (Figure 9a), respectively. The sensor can be recovered quickly when 0.5 mM glucose is dropped into the solution again, showing the good selectivity and repeatability to glucose detection. Generally, the well-balanced physiological level of glucose in the body is about 3 - 8 mM, but the common interfering species in the blood such as uric acid (UA), ascorbic acid (AA) and dopamine (DA) less than 0.1 mM could seriously affect the precise detection of glucose.[47] The interference experiment was carried out by adding 0.1 mM UA, AA or DA into 0.5 mM glucose in the solution, respectively, as shown in Figure 9b. The successive injection of UA and AA has little influence on the detection of glucose, whereas, only a weak response current arises with DA addition in I-T curve, exhibiting the good anti-interference ability to UA, AA and DA. The electrolyte salts of high concentration, such as NaCl, also existing in blood, may seriously poison the electrode during the glucose detection. When 0.1 mM NaCl is added, no any response current caused by NaCl injection appears

in Figure 9c, which recovers to the regular current values once again as the injection of 0.5 mM glucose, indicating that the glucose sensor has a good anti-salt ability. The remarkable selectivity and anti-interference ability of yolk-shell CuO/S-1@mSiO2 based glucose biosensor to various physiological species are mainly attributed to their different oxidation potentials. The electro-oxidation of glucose is occurred at around 0.65 V when $Cu^{2+}$ species are used as the active catalyst. The oxidation potentials of AA, DA, UA are 0.01 V, 0.15 V, 0.27 V, respectively.[48] Fructose has weaker reducing ability than glucose, so its oxidation potential is higher than glucose. Sucrose is a non-reducing sugar. Besides, the shielding and molecular sieving effects of mesoporous silica shell also play an important role in enhancing the anti-interference ability, similar with the high sensitivity and rapid response caused by the enrichment of glucose by mesoporous silica and hollow void as well as the quick removing of gluconic acid by silicalite-1.

Finally, the yolk-shell CuO/S-1@mSiO2 based biosensor was applied to the determination of glucose in real blood serum samples. Here serum sample was firstly diluted by 5 times and then 25 μL diluted sample was added to 25 ml of 100 mM NaOH solution, and the measurement was conducted at an applied potential of 0.65 V. The measured current change was correlated with the glucose concentration according to the calibration curve in Figure 8b, and then compared with the values obtained using a spectrophotometric method performed in the Changhai hospital (Shanghai, China). The data from the fabricated glucose biosensor are 5.27 mM (average value for three measurements), quite close to the result of 5.19 mM determined by a commercial glucose meter, showing a good accuracy along with a high precision, which demonstrates the reliability of yolk-shell CuO/S-1@mSiO2 based non-enzymatic glucose biosensor for the detection of real samples.

## ■ Conclusions

In summary, using a facile sol-gel interface coassembly strategy, we have successfully designed the hierarchical molecular sieve composites with a uniform yolk-shell structure, given the code of CuO/S-1@mSiO2. The crystalline silicalite-1 with hexagonal prism morphology in size of about 250 nm is taken as a core material, which supplies the interface for coating RF resin, and acts as a support for homogeneous dispersion of ultrafine CuO nanoparticles. The thickness of RF layer as a protective transitional shell can be tuned in the range of 20 nm to 65 nm, leading to a hollow void in the final yolk-shell particles. An impregnation grafting method is utilized for functional modification of RF surface with amino groups and then coordination with copper species. A thin silica shell containing disordered mesopores is deposited on the core composites in an ultra-dilute TEOS/CTAB alkaline solution. The yolk-shell CuO/S-1@mSiO2 composites possess high surface area (779 $m^2/g$), pore volume (0.416 $cm^3/g$), and large pore size (4.0 nm), which are constructed as a non-enzymatic biosensor for glucose detection, showing superior sensitivity and selectivity. Under the optimized conditions, the sensor based on yolk-shell CuO/S-1@mSiO2 with Cu content of 1.83% presents some attractive features as wide linear range (5 - 500 μM), high sensitivity (5.5 $\mu A \cdot mM^{-1} \cdot cm^{-2}$), low detection limit (0.17 μM) and outstanding anti-interference abilities. Good accuracy and high precision for the quantification of glucose concentration in human serum samples was also proved. The improved performance as glucose biosensor is primarily attributed to the synergistic effects of three factors: (1) high and homogeneous dispersion of ultrafine CuO nanoparticles on the surface of silicalite-1, showing the spatial accessibility and good catalytic activity to glucose oxidation; (2) the specific yolk-shell structures with hierarchical pores, in which the interconnected mesopores provide a developed diffusion pathway for reactants and electrolyte ions, the large void supplies enough space for the electrocatalytic oxidation of glucose as a nanoreactor, and the micropores in silicalite-1 can selectively remove the oxidation product of gluconic acid; (3) the shielding and molecular sieving effect of mesoporous silica shell, which can significantly prevent the loss of active copper species and selectively control the diffusion of reactants and interfering substances inside the hollow void. All the structural characteristics of the yolk-shell CuO/S-1@mSiO2 composites endow the non-enzymatic glucose biosensor with superior sensitivity, selectivity, stability and anti-interference ability, which possesses the attractive potential to be used as commercialized glucose detector in real physiological system.

## ASSOCIATED CONTENT

### Supporting Information

The Supporting Information is available free of charge via the Internet at http://pubs.acs.org.

## AUTHOR INFORMATION

### Corresponding Author

* (Y. H. Deng) yhdeng@fudan.edu.cn.
* (J. P. Dong) jpdong@shu.edu.cn.

### Author Contributions

All authors have given approval to the final version of the manuscript.

### Notes

The authors declare no competing financial interest..

## ACKNOWLEDGMENT

This work was sponsored by Shanghai Pujiang Program, China (No. 16PJ1401100) and the Shanghai committee of science and technology, China (No. 15ZR1402000), Key Basic Research Program of Science and Technology Commission of Shanghai Municipality (17JC1400100), the NSF of China (21673048), National Youth Top Talent Support Program of National High-level Personnel of Special Support Program (Youth Top-notch Talent Support Program), the state key laboratory of Transducer Technology of China (Grant No. SKT1503).

## REFERENCES


(1) Perez-Ramirez, J.; Christensen, C. H.; Egeblad, K.; Christensen, C. H.; Groen, J. C., Hierarchical zeolites: enhanced utilisation of microporous crystals in catalysis by advances in materials design. *Chem. Soc. Rev.* **2008**, 37, 2530-2542.

(2) Choi, M.; Na, K.; Kim, J.; Sakamoto, Y.; Terasaki, O.; Ryoo, R., Stable single-unit-cell nanosheets of zeolite MFI as active and long-lived catalysts. *Nature* **2009**, 461, 246-249.

(3) Jacobsen, C.; Madsen, C.; Houzvicka, J.; Schmidt, I.; Carlsson, A. Mesoporous zeolite single crystals. *J. Am. Chem. Soc.* **2000**, 122, 7116-7117.

(4) Choi, M.; Cho, H.; Srivastava, R.; Venkatesan, C.; Choi, D.; Ryoo, R., Amphiphilic organosilane-directed synthesis of crystalline zeolite with tunable mesoporosity. *Nat. Mater.* **2006**, 5, 718-723.

(5) Yang, P.; Deng T., Zhao, D.; Feng, P.; Pine, D.; Chmelka, B. F.; Whitesides, G. M.; Stucky, G. D.; Hierarchically ordered oxides. *Science* **1998**, 282, 2244-2246.

(6) Guillet-Nicolas, R.; Popat, A.; Bridot, J. L.; Monteith, G.; Qiao, S. Z.; Kleitz, F., pH-responsive nutraceutical-mesoporous silica nanoconjugates with enhanced colloidal stability. *Angew. Chem. Int. Ed.* **2013**, 52, 2318-2322.

(7) Niu, D.; Ma, Z.; Li, D.; Shi, J.; Synthesis of core-shell structured dual-mesoporous silica spheres with tunable pore size and controllable shell thickness. *J. Am. Chem. Soc.* **2010**, 132, 15144-15147.

(8) Xu, L.; Ren, Y.; Wu, H.; Liu, Y.; Wang, Z.; Zhang, Y.; Xu, J.; Peng, H.; Wu, P., Core/shell-structured TS-1@mesoporous silica-supported Au nanoparticles for selective epoxidation of propylene with $H_2$ and $O_2$. *J. Mater. Chem.* **2011**, 21, 10852-10858.

(9) Vara, M.; Roling, L. T.; Wang, X.; Elnabawy, A. O.; Hood, Z. D.; Chi, M.; Mavrikakis, M.; Xia, Y., Understanding the thermal stability of palladium-platinum core-shell nanocrystals by in-situ transmission electron microscopy and density functional theory. *ACS nano* **2017**, 11, 4571-4581.

(10) Liu, X.; Astruc, D., From galvanic to anti-galvanic synthesis of bimetallic nanoparticles and applications in catalysis, sensing, and materials science. *Adv. Mater.* **2017**, 29, 1605305-1605320.

(11) Zhang, S.; Vlémincq, C.; Ramirez Wong, D.; Magnin, D.; Glinel, K.; Demoustier-Champagne, S.; Jonas, A. M., Nanopapers of layer-by-layer nanotubes. *J. Mater. Chem. B* **2016**, 4, 7651-7661.

(12) Salgueirino-Maceira, V.; Correa-Duarte, M. A.; Farle, M., Manipulation of chemically synthesized FePt nanoparticles in water: core-shell silica/FePt nanocomposites. *Small* **2005**, 1, 1073-1076.

(13) a. Liu, S.; Feng, J.; Bian, X.; Liu, J.; Xu, H.; An, Y., A controlled red phosphorus@Ni–P core@shell nanostructure as an ultralong cycle-life and superior high-rate anode for sodium-ion batteries. *Energy Environ. Sci.* **2017**, 10, 1222-1233; b. Deng, X.; Wei, Z.; Cui, C.; Liu, Q.; Wang, C.; Ma, J., Oxygen-deficient anatase $TiO_2$@C nanospindles with pseudocapacitive contribution for enhancing lithium storage. *J. Mater. Chem. A.* **2018**, 6, 4013-4022.

(14) Yu, J.; Yoon, S.; Lee, Y.; Yoon, K.; Fabrication of bimodal porous silicate with silicalite-1 core/mesoporous shell structures and synthesis of nonspherical carbon and silica nanocases with hollow core/mesoporous shell structures. *J. Phys. Chem. B* **2005**, 109, 7040-7045.

(15) Han, Y.; Pitukmanorom, P.; Zhao, L.; Ying, J. Y., Generalized synthesis of mesoporous shells on zeolite crystals. *Small* **2011**, 7, 326-332.

(16) Qian, X.; Xiong, D.; Asiri, A. M.; Khan, S. B.; Rahman, M. M.; Xu, H.; Zhao, D., A facile route to cage-like mesoporous silica coated ZSM-5 combined with Pt immobilization. *J. Mater. Chem. A* **2013**, 1, 7525-7532.

(17) Qian, X.; Du, J.; Li, B.; Si, M.; Yang, Y.; Hu, Y.; Niu, G.; Zhang, Y.; Xu, H.; Tu, B.; Tang, Y.; Zhao, D., Controllable fabrication of uniform core–shell structured zeolite@SBA-15 composites. *Chem. Sci.* **2011**, 2, 2006-2016.

(18) Yu, H.; Lv, Y.; Ma, K.; Wang, C.; Xue, Z.; Zhao, Y.; Deng, Y.; Dai, Y.; Zhao, D., Synthesis of core-shell structured zeolite-A@mesoporous silica composites for butyraldehyde adsorption. *J. Colloid Interf. Sci.* **2014**, 428, 251-256.

(19) Lv, Y.; Qian, X.; Tu, B.; Zhao, D., Generalized synthesis of core–shell structured nano-zeolite@ordered mesoporous silica composites. *Catal. Today* **2013**, 204, 2-7.

(20) Yue, Q.; Zhang, Y.; Wang, C.; Wang, X.; Sun, Z.; Hou, X.; Zhao, D.; Deng, Y., Magnetic yolk–shell mesoporous silica microspheres with supported Au nanoparticles as recyclable high-performance nanocatalysts. *J. Mater. Chem. A* **2015**, 3, 4586-4594.

(21) Liu, Q.; Cao, Q.; Bi, H.; Liang, C.; Yuan, K.; She, W.; Yang, Y.; Che, R., CoNi@mSiO2@$TiO_2$ and CoNi@Air@$TiO_2$ microspheres with strong wideband microwave absorption. *Adv. Mater.* **2016**, 28, 486-490.

(22) Yao, Y.; He, D. S.; Lin, Y.; Feng, X.; Wang, X.; Yin, P.; Hong, X.; Zhou, G.; Wu, Y.; Li, Y., Modulating fcc and hcp ruthenium on the surface of palladium-copper alloy through tunable lattice mismatch. *Angew. Chem. Int. Ed.* **2016**, 55, 5501-5505.

(23) Hong, Y. J.; Son, M. Y.; Kang, Y. C., One-pot facile synthesis of double-shelled SnO(2) yolk-shell-structured powders by continuous process as anode materials for Li-ion batteries. *Adv. Mater.* **2013**, 25, 2279-2283.

(24) Zhao, M.; Deng, K.; He, L.; Liu, Y.; Li, G.; Zhao, H.; Tang, Z., Core-shell palladium nanoparticle@metal-organic frameworks as multifunctional catalysts for cascade reactions. *J. Am. Chem. Soc.* **2014**, 136, 1738-1741.

(25) Zhou, L.; Kuai, L.; Li, W.; Geng, B., Ion-exchange route to Au-Cu(x)OS yolk-shell nanostructures with porous shells and their ultrasensitive $H_2O_2$ detection. *ACS Appl. Mater. Inter.* **2012**, 4, 6463-6467.

(26) Zhou, Y.; Wang, H.; Gong, M.; Sun, Z.; Cheng, K.; Kong, X.; Guo, Z.; Chen, Q., Yolk-type Au@$Fe_3O_4$@C nanospheres for drug delivery, MRI and two-photon fluorescence imaging. *Dalton T.* **2013**, 42, 9906-9913.

(27) Wang, Y.; Gu, H., Core-shell-type magnetic mesoporous silica nanocomposites for bioimaging and therapeutic agent delivery. *Adv. Mater.* **2015**, 27, 576-585.

(28) Lin, M.; Wang, Y.; Sun, X.; Wang, W.; Chen, L., "Elastic" property of mesoporous silica shell: for dynamic surface enhanced Raman scattering ability monitoring of growing noble metal nanostructures via a simplified spatially confined growth method. *ACS Appl. Mater. Inter.* **2015**, 7, 7516-7525.

(29) Čejka, J.; Centi, G.; Perez-Pariente, J.; Roth, W. J., Zeolite-based materials for novel catalytic applications: opportunities, perspectives and open problems. *Catal. Today* **2012**, 179, 2-15.

(30) Quoc Dung, N.; Patil, D.; Jung, H.; Kim, D., A high-performance nonenzymatic glucose sensor made of CuO-SWCNT nanocomposites. *Biosens. Bioelectron.* **2013**, 42, 280-286.

(31) Chen, A.; Ding, Y.; Yang, Z.; Yang, S., Constructing heterostructure on highly roughened caterpillar-like gold nanotubes with cuprous oxide grains for ultrasensitive and stable nonenzymatic glucose sensor. *Biosens. Bioelectron.* **2015**, 74, 967-973.

(32) Kim, S.; Umar, A.; Hwang, S., Rose-like CuO nanostructures for highly sensitive glucose chemical sensor application. *Ceram. Int.* **2015**, 41, 9468-9475.

(33) Zhu, Z.; Garcia-Gancedo, L.; Chen, C.; Zhu, X.; Xie, H.; Flewitt, A. J.; Milne, W. I., Enzyme-free glucose biosensor based on low density CNT forest grown directly on a Si/$SiO_2$ substrate. *Sensors Actuat.-B Chem.* **2013**, 178, 586-592.

(34) Tominaga, M.; Shimazoe, T.; Nagashima, M.; Kusuda, H.; Kubo, A.; Kuwahara, Y.; Taniguchi, I., Electrocatalytic oxidation

of glucose at gold–silver alloy, silver and gold nanoparticles in an alkaline solution. *J. Electroanal. Chem.* **2006**, 590, 37-46.

(35) Ding, Y.; Wang, Y.; Su, L.; Bellagamba, M.; Zhang, H. Lei, Y., Electrospun $Co_3O_4$ nanofibers for sensitive and selective glucose detection. *Biosens. Bioelectron*, **2010**, 26, 542-548.

(36) Prasad, R.; Gorjizadeh, N.; Rajarao, R.; Sahajwalla, V.; Bhat, B. R., Plant root nodule like nickel-oxide–multi-walled carbon nanotube composites for non-enzymatic glucose sensors. *RSC Adv.* **2015**, 5, 44792-44799.

(37) Reitz, E.; Jia, W.; Gentile, M.; Wang, Y.; Lei, Y., CuO nanospheres based nonenzymatic glucose sensor. *Electroanal.* **2008**, 20, 2482-2486.

(38) Zhang, L.; Li, H.; Ni, Y.; Li, J.; Liao, K.; Zhao, G., Porous cuprous oxide microcubes for non-enzymatic amperometric hydrogen peroxide and glucose sensing. *Electrochem. Commun*. **2009**, 11, 812-815.

(39) Chen, D.; Lu, Y.; Wang, A.; Feng, J.; Huo, T.; Dong, W., Facile synthesis of ultra-long Cu microdendrites for the electrochemical detection of glucose. *J. Solid State Electr.* **2011**, 16, 1313-1321.

(40) Kang, X.; Mai, Z.; Zou, X.; Cai, P. and Mo, J., A sensitive nonenzymatic glucose sensor in alkaline media with a copper nanocluster/multiwall carbon nanotube-modified glassy carbon electrode, *Anal. Biochem.* **2007**, 363, 143-150.

(41) Ramachandran, K.; Babu, K. J.; Kumar, G. G.; Kim, A. R.; Yoo, D. J., One-pot synthesis of graphene supported CuO nanorods for the electrochemical hydrazine sensor applications. *Sci. Adv. Mater.* **2015**, 7, 329-336.

(42) Yang, P.; Xu, Y.; Chen, L.; Wang, X.; Zhang, Q., One-Pot synthesis of monodisperse noble metal @resorcinol-formaldehyde (M@RF) and M@Carbon core-shell nanostructure and their catalytic Applications. *Langmuir* **2015**, 31, 11701-11708.

(43) Rana, S.; Maddila, S.; Jonnalagadda, S. B., Synthesis and characterization of Pd(ii) dispersed over diamine functionalized graphene oxide and its scope as a catalyst for selective oxidation. *Catal. Sci. Technol.* **2015**, 5, 3235-3241.

(44) Ali, Z.; Tian, L.; Zhang, B.; Ali, N.; Khan, M.; Zhang, Q., Synthesis of fibrous and non-fibrous mesoporous silica magnetic yolk–shell microspheres as recyclable supports for immobilization of Candida rugosa lipase. *Enzyme Microb. Tech.* **2017**, 103, 42-52.

(45) Dong, J.; Tian, T.; Ren, L.; Zhang, Y.; Xu, J.; Cheng, X., CuO nanoparticles incorporated in hierarchical MFI zeolite as highly active electrocatalyst for non-enzymatic glucose sensing. *Colloids surfaces: B.,* **2015**, 125, 206-212.

(46) Wang, J.; Zhang, W. D., Fabrication of CuO nanoplatelets for highly sensitive enzyme-free determination of glucose. *Electrochimica Acta* **2011**, 56, 7510-7516.

(47) Zhang, P.; Zhang, L.; Zhao, G.; Feng, F., A highly sensitive nonenzymatic glucose sensor based on CuO nanowires. *Microchimica Acta* **2011**, 176, 411-417.

(48) Zhang, X. J.; Dong, J. P.; Qian' X. Z.; Zhao, C. J., One-pot synthesis of an RGO/ZnO nanocomposite on zinc foil and its excellent performance for the nonenzymatic sensing of xanthine. *Sensors Actuat.-B Chem.*, **2015**, 221, 528-536.

## Graphical abstract

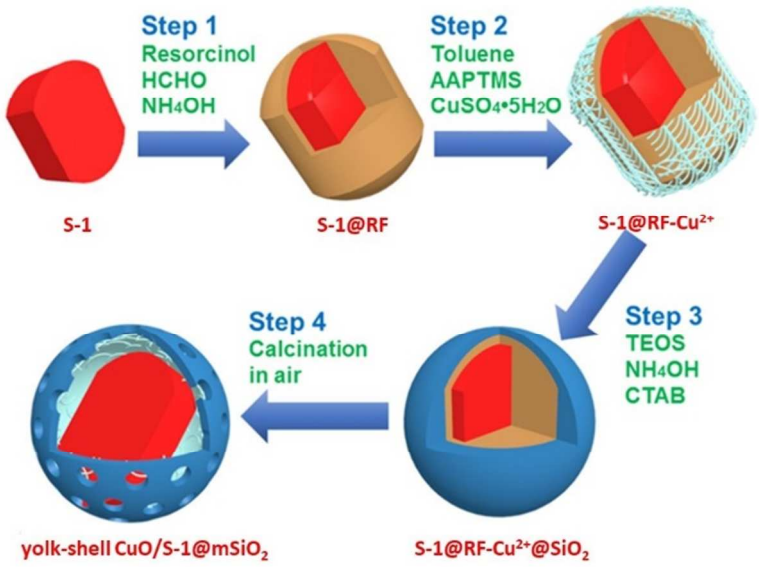


The novel yolk-shell CuO/silicalite-1@mSiO2 composites were prepared through the multistep sol-gel interface coassembly strategy, which are composed of a core of silicalite-1 single crystal, highly dispersed ultrafine CuO nanoparticles, large hollow void and a shell of mesoporous silica. When constructed as a non-enzymatic glucose biosensor, the multifunctional hierarchical material exhibits the excellent electrocatalytic performance in glucose detection, such as high sensitivity, low detection limit, good selectivity and strong anti-interference ability.